miRNA-independent function of long noncoding pri-miRNA loci

Daniel He[a,b,c], David Wu[a,b,d], Soren Muller[a,1], Lin Wang[a], Parna Saha[a,b,e], Sajad Hamid Ahanger[a,b,e], Siyuan John Liu[a,b,d], Miao Cui[a,b], Sung Jun Hong[a,b,c], Miten Jain[f,g], Hugh E. Olson[f,g], Mark Akeson[f,g], Joseph F. Costello[a], Aaron Diaz[a], and Daniel A. Lim[a,b,e,2]

[a]Department of Neurological Surgery, Biomedical Sciences Graduate Program, University of California, San Francisco, CA 94143; [b]Eli and Edythe Broad Center of Regeneration Medicine and Stem Cell Research, Biomedical Sciences Graduate Program, University of California, San Francisco, CA 94143; [c]Developmental and Stem Cell Biology Graduate Program, Biomedical Sciences Graduate Program, University of California, San Francisco, CA 94143; [d]Medical Scientist Training Program, Biomedical Sciences Graduate Program, University of California, San Francisco, CA 94143; [e]Department of Surgery, San Francisco Veterans Affairs Medical Center, San Francisco, CA 94121; [f]Department of Biomolecular Engineering, University of California, Santa Cruz, CA 95064; and [g]UCSC Genomics Institute, University of California, Santa Cruz, CA 95064

Edited by Joan A. Steitz, Yale University, New Haven, CT, and approved February 14, 2021 (received for review August 19, 2020)

Among the large, diverse set of mammalian long noncoding RNAs (lncRNAs), long noncoding primary microRNAs (lnc-pri-miRNAs) are those that host miRNAs. Whether lnc-pri-miRNA loci have important biological function independent of their cognate miRNAs is poorly understood. From a genome-scale lncRNA screen, lnc-pri-miRNA loci were enriched for function in cell proliferation, and in glioblastoma (i.e., GBM) cells with *DGCR8* or *DROSHA* knockdown, lnc-pri-miRNA screen hits still regulated cell growth. To molecularly dissect the function of a lnc-pri-miRNA locus, we studied *LOC646329* (also known as *MIR29HG*), which hosts the miR-29a/b1 cluster. In GBM cells, *LOC646329* knockdown reduced miR-29a/b1 levels, and these cells exhibited decreased growth. However, genetic deletion of the miR-29a/b1 cluster (*LOC646329-miR29Δ*) did not decrease cell growth, while knockdown of *LOC646329-miR29Δ* transcripts reduced cell proliferation. The miR-29a/b1–independent activity of *LOC646329* corresponded to enhancer-like activation of a neighboring oncogene (*MKLN1*), regulating cell propagation. The *LOC646329* locus interacts with the *MKLN1* promoter, and antisense oligonucleotide knockdown of the lncRNA disrupts these interactions and reduces the enhancer-like activity. More broadly, analysis of genome-wide data from multiple human cell types showed that lnc-pri-miRNA loci are significantly enriched for DNA looping interactions with gene promoters as well as genomic and epigenetic characteristics of transcriptional enhancers. Functional studies of additional lnc-pri-miRNA loci demonstrated cognate miRNA-independent enhancer-like activity. Together, these data demonstrate that lnc-pri-miRNA loci can regulate cell biology via both miRNA-dependent and miRNA-independent mechanisms.

lncRNA | lnc-pri-miRNA | miRNA | host gene

An increasing number of long noncoding RNAs (lncRNAs)—transcripts longer than 200 nucleotides (nt) that have little evidence of protein coding potential—have been discovered to have important biological roles, functioning via diverse molecular mechanisms (1, 2). Given their broad definition, lncRNAs are very heterogeneous, and based on differences in transcript structure, processing, and the local genomic context, several major lncRNA subclasses can be defined (3). One major lncRNA subclass is comprised of long noncoding primary microRNAs (lnc-pri-miRNAs), transcripts that are processed to produce microRNAs (miRNAs) (4, 5). miRNAs are short (~22 nt) noncoding transcripts that regulate gene expression posttranscriptionally by promoting mRNA degradation and/or inhibiting translation (6). miRNAs are generally derived from primary transcripts termed primary miRNAs (pri-miRNAs), and while many pri-miRNAs are transcribed from protein coding genes, ~600 miRNAs are produced from lnc-pri-miRNAs (5, 7).

Emerging evidence indicates that lnc-pri-miRNAs can have important roles in development and disease (8–12), but it is unclear whether lnc-pri-miRNA function primarily relates to the miRNAs that are produced. Although certain studies provide evidence for lnc-pri-miRNA function that appears miRNA-independent (10, 11), other studies of these same lnc-pri-miRNAs relate function primarily to their cognate miRNAs (8, 12).

In a genome-scale CRISPR interference (CRISPRi) screen of lncRNAs, many lnc-pri-miRNA loci regulate cell proliferation (13), and we initially presumed that these lnc-pri-miRNAs functioned primarily through miRNA-based mechanisms. However, in glioblastoma multiforme (GBM) cells with knockdown of *DGCR8* or *DROSHA*—key components of miRNA processing—all of the lnc-pri-miRNA screen hit loci still strongly regulated cell proliferation. To more incisively dissect lnc-pri-miRNA function, we studied *LOC646329*, which hosts miR-29a/b1. Using multiple, complementary methods, we found that *LOC646329* can regulate GBM cell growth independent of its cognate miRNAs, and this miRNA-independent activity corresponded to enhancer-like activation of a neighboring oncogene. To explore whether additional lnc-pri-miRNA loci also have evidence of enhancer-like

Significance

The human genome contains many thousands of genes that produce a large diversity of long noncoding RNAs (lncRNAs). Some lncRNA genes produce microRNAs (miRNAs), which are regulators of protein expression. It has been unclear whether lncRNA genes that produce miRNAs, termed lnc-pri-miRNAs, have important function independent of their miRNAs. We find multiple lnc-pri-miRNA genes that regulate cell proliferation even when miRNA production machinery is knocked down. lnc-pri-miRNA *LOC646329* produces miR-29a/b1, and the function of *LOC646329* in cell proliferation can be genetically and phenotypically separated from its cognate miRNAs. The miRNA-independent function of *LOC646329* and other lnc-pri-miRNAs relates to their activation of genes in physical proximity. These results shed light on the function and intermingled complexity of the noncoding genome.

Author contributions: D.H., M.C., and D.A.L. designed research; D.H., P.S., S.H.A., and M.C. performed research; D.H., D.W., S.M., L.W., S.J.L., M.J., H.E.O., M.A., J.F.C., and A.D. contributed new reagents/analytic tools; D.H., D.W., S.M., L.W., P.S., S.H.A., S.J.L., S.J.H., M.J., H.E.O., M.A., and A.D. analyzed data; and D.H. wrote the paper.

The authors declare no competing interest.

This article is a PNAS Direct Submission.

[1]Present address: Department of Bioinformatics and Computational Biology, Genentech, South San Francisco, CA 94080.

[2]To whom correspondence may be addressed. Email: daniel.lim@ucsf.edu.

This article contains supporting information online at https://www.pnas.org/lookup/suppl/doi:10.1073/pnas.2017562118/-/DCSupplemental.

Published March 23, 2021.

activity, we analyzed genome-wide data from multiple human cell types, finding that lnc-pri-miRNA loci were significantly enriched for key characteristics of transcriptional enhancers, and CRISPRi targeting demonstrated enhancer-like function of multiple lnc-pri-miRNA loci.

Results

lnc-pri-miRNA Loci Regulate Cell Proliferation in Cells with Microprocessor Knockdown. In a genome-scale screen of lncRNA function (13), CRISPRi was used to target a total of 5,689 lncRNA loci expressed in U87 GBM cells. Of the 65 hits, 5 targeted the transcription start site (TSS) of 4 different lnc-pri-miRNA loci, representing a ~6.6-fold enrichment of function ($P = 0.001$) over that of other lncRNAs (*SI Appendix*, Fig. S1 *A* and *B*). Similarly, lnc-pri-miRNAs were also significantly enriched for function in MDAMB231 cells, MCF7, and induced pluripotent stem cells (*SI Appendix*, Fig. S1*C*). Using internally controlled growth assays (13) (*Methods*), we validated the four lnc-pri-miRNA screen hits with individual CRISPRi single guide RNAs (sgRNAs) in U87-dCas9-KBAB cells (Fig. 1 *A* and *B* and *SI Appendix*, Fig. S2 *A* and *B*).

To test whether the cell proliferation function of these lnc-pri-miRNA loci requires miRNA production, we generated U87 cells with stable CRISPRi-mediated knockdown of either *DGCR8* or *DROSHA* (Fig. 1*C*), key Microprocessor enzymes required for miRNA production (*SI Appendix*, Fig. S2*C*) (14, 15), and neither *DGCR8* nor *DROSHA* knockdown altered the propagation of U87 cells (Fig. 1*D*). Despite knockdown of *DGCR8* or *DROSHA*, the cell proliferation phenotype of CRISPRi targeting of the four lnc-pri-miRNAs was still observed, even in cells that exhibited no further reduction in mature miRNA levels as seen with miR-29a (Fig. 1*E* and *SI Appendix*, Fig. S2 *C* and *D*). These results suggest that lnc-pri-miRNA loci have important function that is independent of normal Microprocessor function.

***LOC646329* Knockdown Increases Apoptosis and Reduces Proliferation of GBM Cells.** To more directly test whether a lnc-pri-miRNA locus can regulate cell proliferation independent of its cognate miRNA, we focused on one of the lnc-pri-miRNA hits, *LOC646329*. *LOC646329* encodes a spliced lnc-pri-miRNA transcript (GenBank accession no. EU154353) with the miR-29a/b1 cluster located between exon 3 and 4 (16, 17). Using long-read single-molecule Oxford Nanopore direct RNA sequencing (RNA-seq) and Illumina RNA-seq, we confirmed the production of transcripts from the *LOC646329* TSS that span the miR-29a/b1 cluster (Fig. 2*A*). Cell fractionation as well as fluorescent in situ hybridization (FISH) analysis demonstrated *LOC646329* to be a nuclear-enriched lncRNA (*SI Appendix*, Fig. S3 *A* and *B*). Consistent

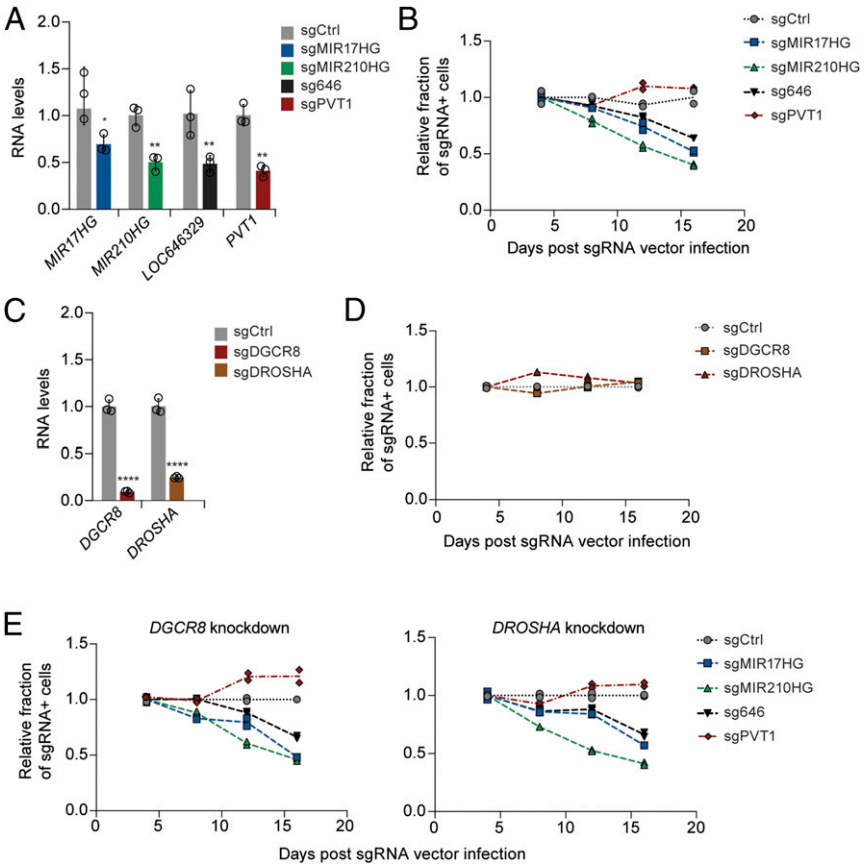

Fig. 1. lnc-pri-miRNA loci can regulate cell proliferation in cells with Microprocessor knockdown. (*A*) RT-qPCR quantification of CRISPRi knockdown in U87 dCas9-KRAB cells (*$P < 0.05$, **$P < 0.01$, unpaired two-sample *t* test). (*B*) Internally controlled growth assays performed with sgRNAs targeting lnc-pri-miRNA loci in U87 dCas9-KRAB cells. sgRNA-expressing cells were quantified by flow cytometry and represented as the fraction observed at 4 d after sgRNA vector infection. Each sgRNA vector infection was performed in biological duplicates, as shown by individual points on the graph. (*C*) RT-qPCR quantification of CRISPRi-mediated knockdown of *DGCR8* and *DROSHA* (****$P < 0.0001$, unpaired two-sample *t* test). (*D*) Internally controlled growth assays of U87 cells with *DGCR8* or *DROSHA* knockdown. Each sgRNA vector infection was performed in biological duplicates, as shown by individual points on the graph. (*E*) Internally controlled growth assays performed with sgRNAs targeting lnc-pri-miRNA loci in U87 dCas9-KRAB cells with *DGCR8* or *DROSHA* knockdown. Each sgRNA vector infection was performed in biological duplicates, as shown by individual points on the graph.

with *LOC646329* serving as a lnc-pri-miRNA for miR-29a/b1 (16, 17), targeting CRISPRi repressive complexes to the *LOC646329* TSS, which is ~36 kb upstream of the miR-29a/b1 cluster, reduced levels of both miR-29a and miR-29b1 (Fig. 2 *B* and *C* and *SI Appendix*, Fig. S3*C*).

CRISPRi-mediated knockdown of *LOC646329* decreased the propagation of U87 GBM cells (*SI Appendix*, Fig. S3*D*), increasing apoptosis as determined by immunocytochemistry (ICC) analysis for activated caspase 3 and decreasing proliferative cells as measured by expression of Ki67 (Fig. 2*D*). In

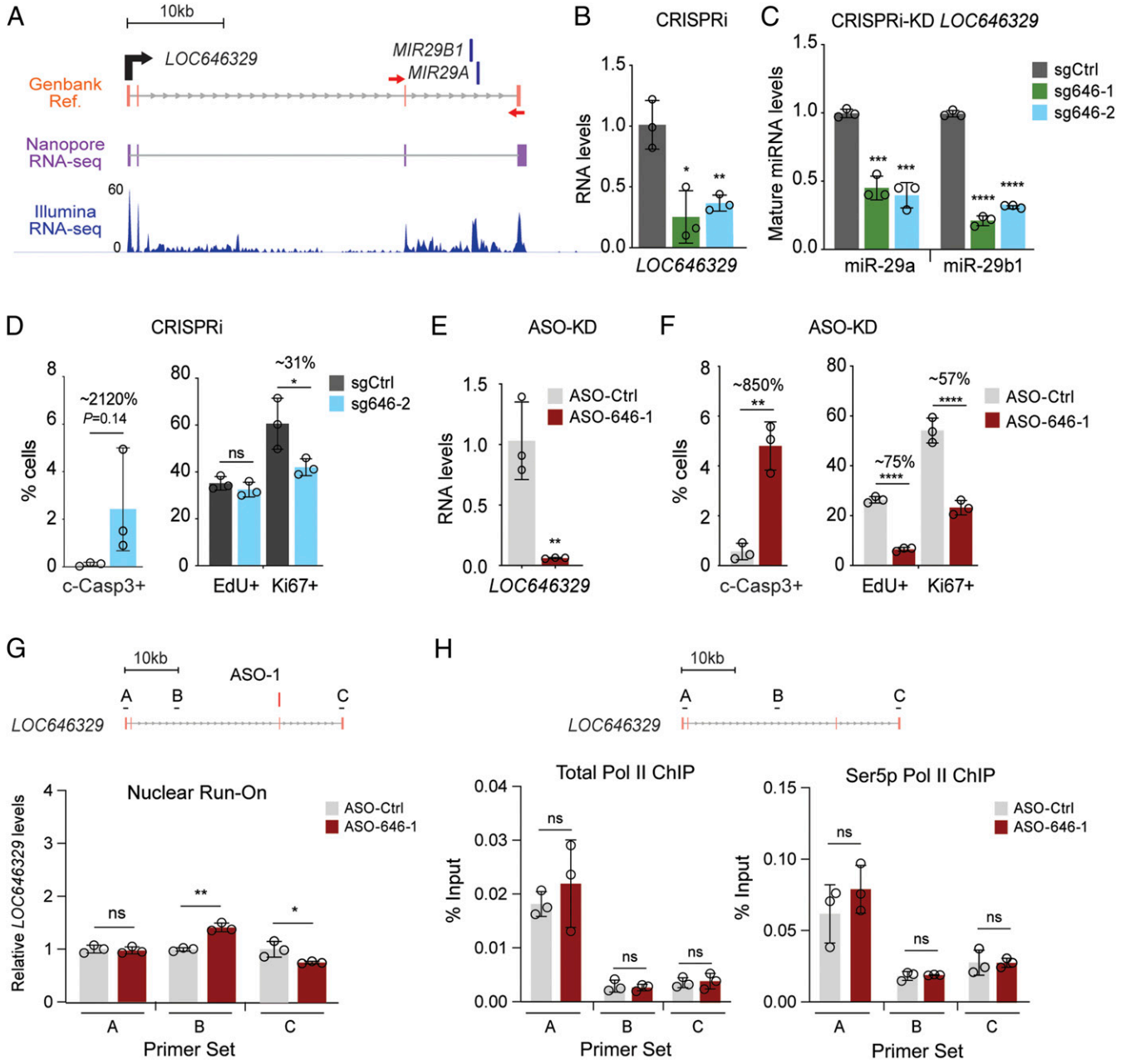

Fig. 2. *LOC646329* produces miR-29a/b1 and is required for U87 cell propagation. (*A*) GenBank reference (EU154353) of *LOC646329* aligned with long-read, single-molecule Oxford Nanopore direct RNA-seq reads (purple) and Illumina RNA-seq reads (blue) in U87 cells. Red arrows indicate exon 3-4 junction–spanning qPCR primers. (*B*) RT-qPCR quantification of *LOC646329* in U87-dCas9-KRAB cells upon CRISPRi with two independent sgRNAs targeting the TSS of *LOC646329* relative to control Gal4 sgRNA (*$P < 0.05$, **$P < 0.01$, unpaired two-sample *t* test). (*C*) RT-qPCR quantification of mature miR-29a and miR-29b after CRISPRi-mediated knockdown of *LOC646329* ($n = 3$ biological replicates per condition). Gal4 sgRNA is used as control (***$P < 0.001$, ****$P < 0.0001$, unpaired two-sample *t* test). (*D*) Quantification of ICC of U87-dCas9-KRAB cells 1 wk post CRISPRi-mediated *LOC646329* knockdown ($n = 3$ biological replicates per condition; ns, not significant; *$P < 0.05$, unpaired two-sample *t* test). (*E*) RT-qPCR quantification of *LOC646329* 48 h post ASO transfection (**$P < 0.01$, unpaired two-sample *t* test). (*F*) Quantification of ICC of U87 cells 48 h post ASO-mediated *LOC646329* knockdown ($n = 3$ biological replicates per condition; *$P < 0.05$, **$P < 0.01$, ****$P < 0.0001$, unpaired two-sample *t* test). (*G*) RT-qPCR quantification of *LOC646329* nascent transcript levels in NRO experiments in U87 cells with and without *LOC646329* ASO-mediated knockdown. Primer sets and locations are indicated by the schematic above (*$P < 0.05$, **$P < 0.01$; ns, not significant; unpaired two-sample *t* test). (*H*) ChIP analysis with antibodies to total RNA Pol II (*Left*) and RNA Pol II Ser5p (*Right*) using qPCR primers indicated in the schematic above.

contrast, *LOC646329* knockdown did not decrease the propagation of HeLa cervical cancer cells (*SI Appendix*, Fig. S4 *A–C*) or normal human astrocytes (*SI Appendix*, Fig. S4 *D–F*), consistent with most essential lncRNAs having cell type-specific function (13).

CRISPRi represses transcription by sterically blocking RNA polymerase (RNA Pol) and inducing local heterochromatinization (18, 19). To decrease *LOC646329* levels with an orthogonal method, targeting the RNA transcript itself, we used antisense oligonucleotides (ASOs) that trigger RNA degradation via a ribonuclease H-based mechanism. While ASOs targeting the nascent transcript or near the 5′ end of RNA can trigger premature transcriptional termination (20, 21), we used ASOs designed to the distal 3′ end of *LOC646329*, which is at least 35,771 bp from the TSS (*SI Appendix*, Fig. S3*E*). ASO-mediated *LOC646329* knockdown significantly reduced FISH signal (*SI Appendix*, Fig. S3 *F* and *G*) and strongly reduced U87 cell propagation as compared to the negative control ASO (Fig. 2*E* and *SI Appendix*, Fig. S5 *A* and *B*), increasing apoptosis and decreasing proliferation as determined by ICC analysis for the incorporation of 5-ethynyl-2′-deoxyuridine (EdU) and Ki67 expression (Fig. 2*F* and *SI Appendix*, Fig. S5 *B* and *C*). Although *LOC646329* ASO-1 and ASO-2 produce a similar phenotype (Fig. 2*F* and *SI Appendix*, Fig. S5*C*), nuclear run-on (NRO) experiments to assess nascent transcription suggest ASO-2 can induce premature transcriptional termination (*SI Appendix*, Fig. S5*D*), while ASO-1 only modestly reduces (~24%) nascent transcripts observed at the distal 3′ end (Fig. 2*G*). Chromatin immunoprecipitation (ChIP) analysis of total Pol II as well as RNA Pol II with serine 5 phosphorylation (S5P)—a posttranslational modification required for robust initiation and elongation (22)—did not reveal a significant difference in Pol II occupancy throughout the gene body (Fig. 2*H*), providing further evidence that ASO-1 does not disrupt transcription through the 5′ regions of *LOC646329*.

Deletion of miR-29a/b1 Does Not Decrease Cell Growth. Given that *LOC646329* is a lnc-pri-miRNA for miR-29a and miR-29b1, we investigated whether the growth-inhibitory effect of *LOC646329* knockdown in GBM cells was due to decreased miR-29a/b1 activity. First, we used a miR-29 sponge construct (*SI Appendix*, Fig. S6*A*) to reduce miR-29a/b1 levels and activity (*SI Appendix*, Fig. S6*B*). While U87 cells expressing the miR-29 sponge did not exhibit a growth defect (*SI Appendix*, Fig. S6 *C* and *D*), we considered the possibility that the sponge construct did not fully inhibit miR-29 activity. Thus, we next used CRISPR-Cas9 to genetically delete miR-29a/b1 from *LOC646329*. U87 cells expressing the Cas9 nuclease were transfected to transiently express pairs of sgRNAs that flank the miR-29a/b1 cluster (Fig. 3*A*). Cells were then clonally isolated, and miR-29a/b1–knockout cells (*LOC646329-miR29Δ*) were confirmed by PCR genotyping and Sanger sequencing (*SI Appendix*, Fig. S7*A*). In *LOC646329-miR29Δ* cells, expression of miR-29a/b1 was essentially abolished as assessed by RT-qPCR analysis and miRNA sequencing (Fig. 3*B* and *SI Appendix*, Fig. S7*B*), resulting in the derepression (Fisher's exact test, $P = 1.9^{-35}$) of known miR-29 target genes (*SI Appendix*, Fig. S7 *C* and *D* and Dataset S1). These miR-29 target genes were enriched for regulation of extracellular matrix (ECM) organization and unfolded protein response (*SI Appendix*, Fig. S7*E*), consistent with miR-29's role in ECM remodeling (23), and apoptosis (16, 24, 25). miR-29b2/c—miRNA family members that are encoded from a locus on a different chromosome—were not detected in either wild-type or *LOC646329-miR29Δ* U87 cells (*SI Appendix*, Fig. S7*B*).

In all three U87 cell clones (clones 15, 18, and 40) with *LOC646329-miR29Δ*, cellular propagation was not decreased as compared to nondeleted controls. Surprisingly, clones 18 and 40 exhibited a faster cell cycle (*SI Appendix*, Fig. S8 *A* and *B*), resulting in greater numbers of cells (1.58- to 1.74-fold increase) over 15 d of culture (*SI Appendix*, Fig. S8*C*). Furthermore, the clones did not exhibit an increase in apoptosis, and more Ki67$^+$ cells were observed in clones 18 and 40 (Fig. 3*C*). Taken together, these data indicate that the decrease in U87 cell propagation observed with CRISPRi- (*SI Appendix*, Fig. S3*D*) or ASO-mediated *LOC646329* knockdown (*SI Appendix*, Fig. S5 *A* and *B*) does not solely relate to decreased miR-29a/b1 levels.

***LOC646329* Has Cellular Function Independent of Its Cognate miRNAs.** In cells deleted for miR-29a/b1, transcripts from *LOC646329-miR29Δ* gene were detected at increased levels as compared to wild-type *LOC646329* (up to ~33-fold; Fig. 3*D*), accumulating as focal "clouds" in the nucleus, as observed by in situ hybridization (Fig. 3*E*). The increased levels of *LOC646329-miR29Δ* correlated with a fourfold increase in transcript half-life (*SI Appendix*, Fig. S8*D*), and ChIP analysis revealed increased levels of RNA Pol II as well as RNA Pol II S5P at the TSS of *LOC646329-miR29Δ* (*SI Appendix*, Fig. S8*E*). Thus, as compared to the wild-type locus, *LOC646329-miR29Δ* produces lncRNA transcripts with increased stability from a TSS with more RNA Pol II activity.

We next investigated whether *LOC646329* is required for cell proliferation independent of its production of miR-29a/b1. Using the same ASOs effective for *LOC646329* depletion, we knocked down the *LOC646329-miR29Δ* transcripts in U87 cells (Fig. 4*A* and *SI Appendix*, Fig. S9*A*). Interestingly, knockdown of *LOC646329-miR29Δ* did not increase apoptosis (Fig. 4*B* and *SI Appendix*, Fig. S9*B*), as was observed with ASO-mediated knockdown of *LOC646329* (Fig. 2*F*). However, in all three clones with miR-29a/b1-deletion, knockdown of *LOC646329-miR29Δ* still strongly reduced cell proliferation (Fig. 4*B* and *SI Appendix*, Fig. S9*B*). U87 cells with *LOC646329-miR29Δ* knockdown resulted in the differential expression of 290 genes (108 up-regulated, 182 down-regulated) that had significant overlap (n = 256; 88%; Dataset S2) with gene expression changes observed with *LOC646329* knockdown (*SI Appendix*, Fig. S9*C* and Dataset S3). This set of common differentially expressed genes are enriched for regulation of sodium ion transmembrane transport and DNA repair (*SI Appendix*, Fig. S9*D*). Thus, the *LOC646329-miR29Δ* transcript, which no longer serves as a precursor of miR-29a/b1, is required for robust U87 cell proliferation.

To further test whether *LOC646329* regulates cell proliferation independent of its production of its cognate miRNAs, we introduced miR-29a/b1 into U87 cells with or without knockdown of its lnc-pri-miRNA transcript (*SI Appendix*, Fig. S10 *A–C*). In control U87 cells without *LOC646329* knockdown, transfection of miR-29a/b1 significantly increased apoptosis without adversely affecting EdU incorporation or Ki67 expression (*SI Appendix*, Fig. S10 *A* and *C*), consistent with the proapoptotic effect of miR-29 overexpression (16, 24, 25). In cells with *LOC646329* knockdown, the reintroduction of exogenous miR-29a/b1 partially reversed the apoptosis phenotype, but the cell proliferation defect was not changed (*SI Appendix*, Fig. S10 *B* and *C*). Thus, the levels of miR-29 activity (in cells with or without *LOC646329* knockdown) can regulate apoptosis without adversely affecting measures of cell proliferation. Transfection of miR-29a/b1 did not reduce levels of *LOC646329* (*SI Appendix*, Fig. S10*A*), contrary to the recent observation that miR-29b1 can target *LOC646329* in colorectal cancer cells (26). These data further support the concept that *LOC646329* has critical cellular function that is separable from the function that its cognate miRNAs play in apoptosis.

The *LOC646329* Locus Contains Transcriptional Enhancer Activity. Some lncRNAs can regulate the expression of gene neighbors (20, 27–31). Within a 1-MB genomic window around *LOC646329*, the expression of *MKLN1* and *linc-PINT* was decreased by both ASO- (Fig. 4*C* and *SI Appendix*, Fig. S11 *A* and *B*) and CRISPRi-mediated knockdown of *LOC646329* (*SI Appendix*, Fig. S11*C*). Of note, *MKLN1*, a putative oncogene in human glioma (32), was

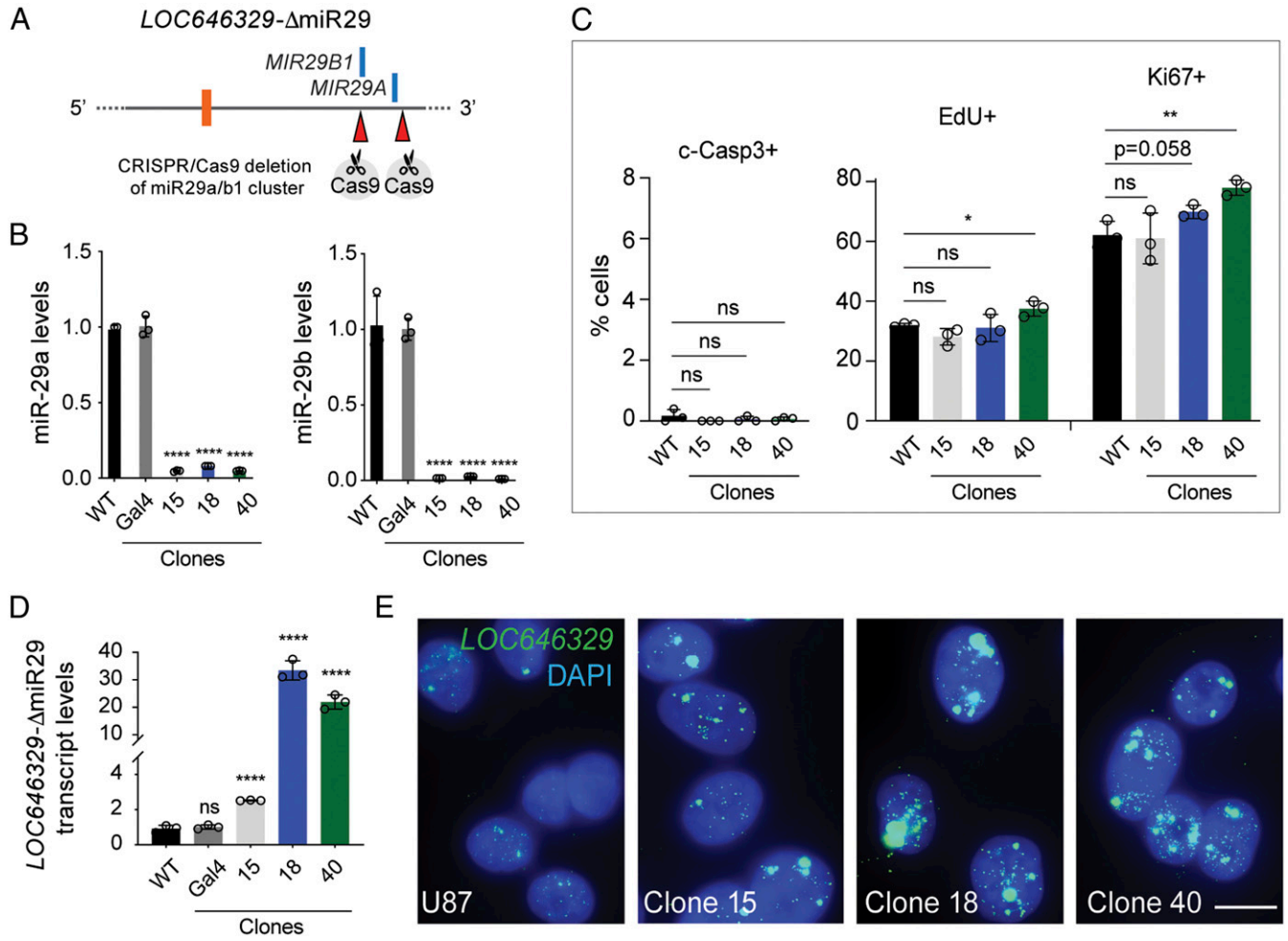

Fig. 3. Deletion of miR-29a/b1 does not decrease cell growth. (*A*) Schematic of genetic removal of miR-29a/b1 using CRISPR-Cas9. (*B*) RT-qPCR quantification of mature miR-29a and miR-29b levels in CRISPR-edited clones and controls ($n = 3$ biological replicates per condition; ****$P < 0.0001$, unpaired two-sample *t* test). (*C*) Quantification of ICC in wild-type and CRISPR-edited clones ($n = 3$ biological replicates per condition; ns, not significant; *$P < 0.05$, **$P < 0.01$, unpaired two-sample *t* test). (*D*) RT-qPCR of *LOC646329* in CRISPR-edited clones and controls ($n = 3$ biological replicates per condition; ns, not significant; ****$P < 0.0001$, unpaired two-sample *t* test). (*E*) FISH of *LOC646329* (green) in U87 cells, clone 15, clone 18, and clone 40. Nuclei are counterstained with DAPI (blue). (Scale bars, 8 mM.)

significantly decreased as early as 4 h post ASO transfection in U87 cells, suggesting direct regulation by *LOC646329* (*SI Appendix*, Fig. S11*D*). To ensure dCas9-KRAB did not directly affect *MKLN1* in the CRISPRi knockdown of *LOC646329*, we conducted H3K9me3 ChIP-seq analysis and found H3K9me3 significantly gained only at the *LOC646329* promoter (*SI Appendix*, Fig. S12*A*), but not at the *MKLN1* promoter or any other site genome-wide (*SI Appendix*, Fig. S12*B*). Furthermore, ASO-mediated knockdown of *MKLN1* decreased U87 cell propagation (Fig. 4 *D* and *E* and *SI Appendix*, Fig. S11*E*). Double knockdown of both *LOC646329* and *MKLN1* (*SI Appendix*, Fig. S13*A*) did not result in a significant difference in apoptosis or proliferation as compared to *LOC646329* knockdown alone (*SI Appendix*, Fig. S13*B*), suggesting that *LOC646329* is epistatic to *MKLN1*. Although knockdown of *LOC646329* also resulted in a reduction of *MKLN1* levels in both HeLa and normal human astrocytes (*SI Appendix*, Fig. S14 *A* and *C*), ASO-mediated knockdown of *MKLN1* in HeLa or normal human astrocytes did not decrease cell propagation as determined by ICC analysis (*SI Appendix*, Fig. S14 *B* and *D*).

Analysis of genome-wide chromosome conformation capture (Hi-C) data generated from human fetal brain tissue (33) revealed increased DNA–DNA interaction frequencies between the *LOC646329* locus and *MKLN1*/*linc-PINT*, which are ~200 kb apart, with *MKLN1* and *linc-PINT* having overlapping but divergent promoters. By integrating seven genome-wide databases, GeneHancer (34) yields a map of high-confidence "double-elite" enhancers, one of which is *LOC646329*, shown as an enhancer interacting with the *MKLN1*/*linc-PINT* promoters (Fig. 4*F*). To confirm these interactions between *LOC646329* and *MKLN1*/*linc-PINT*, we performed chromosome conformation capture (3C) followed by qPCR (Fig. 4*G* and *SI Appendix*, Fig. S15). ASO-mediated knockdown of *LOC646329* decreased the observed *LOC646329–MKLN1* interaction frequency (Fig. 4*G* and *SI Appendix*, Fig. S15).

Given the observation of these enhancer-like DNA interactions, we next investigated whether sequences from the *LOC646329* locus possess enhancer-like activity. In a plasmid-based enhancer-reporter assay, a 1,992-bp fragment from the 5′ end of *LOC646329* increased the basal expression of the reporter gene by ~15 fold, while the TSS regions from 3 other lncRNAs with function in U87 cells (13) exhibited little to no enhancer-like activity (Fig. 4*H*). This increase in reporter gene expression was not likely due to transcriptional readthrough from the *LOC646329* TSS, as the DNA fragment was cloned into the reporter construct in the reverse

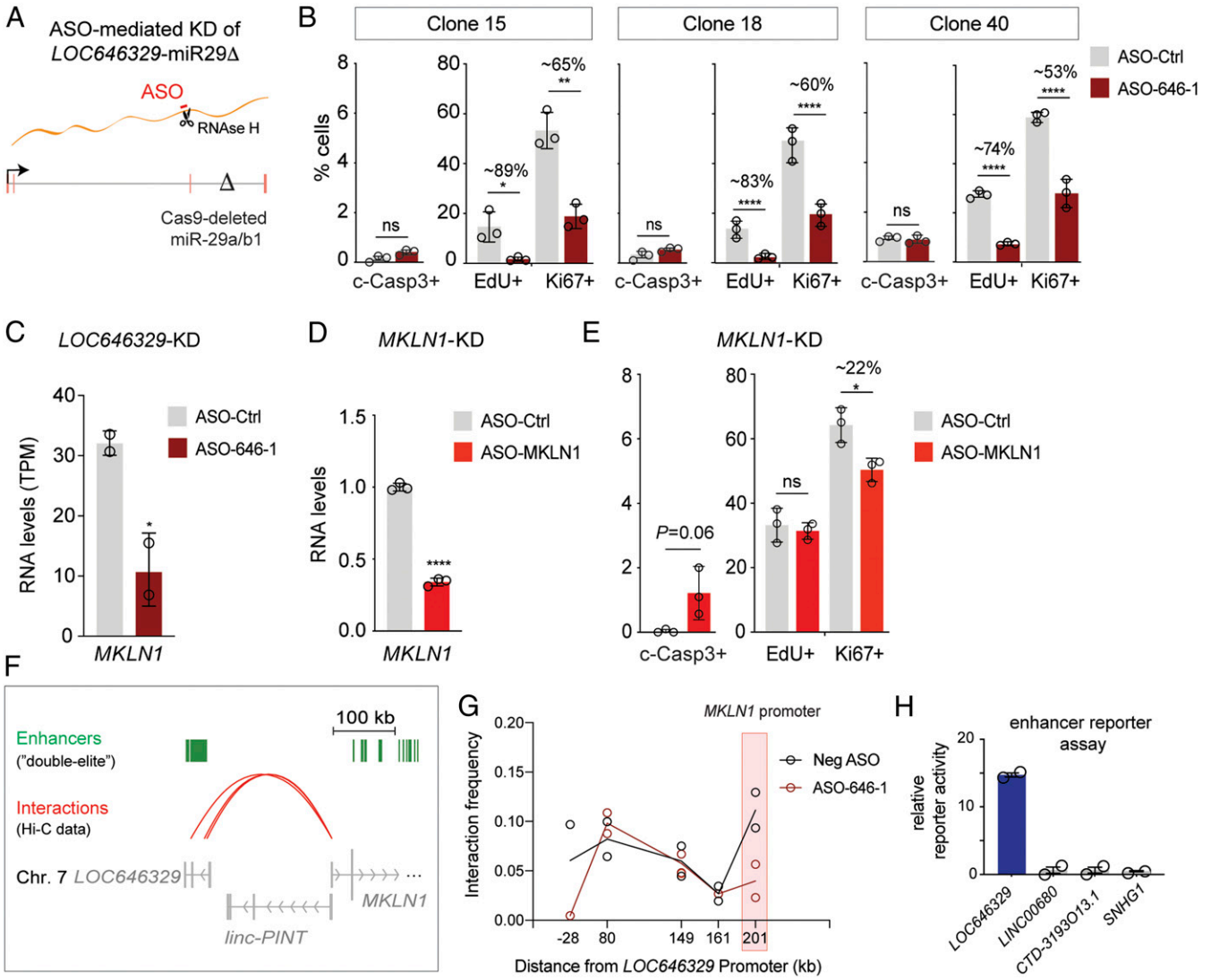

Fig. 4. *LOC646329* regulates cell proliferation independent of miR29a/b1 and exhibits enhancer-like activity. (*A*) Schematic of ASO degradation (targeting exon 3) of U87 *LOC646329-miR29Δ*. (*B*) ICC quantification of U87 *LOC646329-miR29Δ* cells 48 h post ASO-mediated *LOC646329* knockdown. ns, not significant (*$P < 0.05$, **$P < 0.01$, ***$P < 0.001$, ****$P < 0.0001$, two-sample unpaired *t* test). (*C*) Quantification of *MKLN1*-normalized read counts in transcripts per million (TPM) from RNA-seq 24 h after ASO-mediated *LOC646329* knockdown. Asterisk indicates significant difference as determined by the likelihood ratio test. (*D*) Quantification of *MKLN1* levels 48 h after transfection of ASOs. (*E*) Quantification of ICC of U87 cells 48 h post ASO-mediated *MKLN1* knockdown. ns, not significant (*$P < 0.05$, unpaired two-sample *t* test). (*F*) Analysis of GeneHancer high-confidence enhancers and physical interactions between *LOC646329* and *MKLN1*/linc-*PINT*. (*G*) The 3C-qPCR analysis in U87 cells with *LOC646329* promoter as bait. Red highlighted region indicates the *MKLN1* promoter region. Data represented by negative control ASO-treated U87 cells are shown in black, while data represented by ASO-1–mediated *LOC646329* knockdown are shown in red. Each region is analyzed in duplicate, with each dot representing an individual replicate. (*H*) Enhancer reporter activity of the promoter region of four functional lncRNAs listed on the *x* axis.

orientation (*SI Appendix*, Fig. S16*A*). Furthermore, ASOs that target the partial *LOC646329* transcript produced by the reporter construct (*SI Appendix*, Fig. S16 *B* and *C*) decreased enhancer-reporter activity (*SI Appendix*, Fig. S16 *D* and *E*). Thus, *LOC646329* contains sequences with potent enhancer-like activity and exhibited genomic interactions with *MKLN1*, a coding gene required for robust proliferation of U87 GBM cells.

lnc-pri-miRNA Loci Are Enriched for Physical Interactions with Gene Promoters and Enhancer Characteristics. We next explored whether lnc-pri-miRNA loci as a group have evidence of enhancer-like function. By using PSYCHIC (35) to analyze Hi-C data from seven different human cell lines representing all three germ layers (36) (*SI Appendix*, Fig. S17*A*), we found that lnc-pri-miRNA loci had an approximate threefold increase in physical proximity with gene promoters as compared to the broader set of lncRNAs (Fig. 5*A*). Analysis of Pol II occupancy at promoter regions did not reveal significant differences at lnc-pri-miRNA loci as compared to other lncRNAs (*SI Appendix*, Fig. S18), suggesting that differences in Pol II enrichment do not underlie the increased proximity of lnc-pri-miRNA loci and coding genes. When compared to the broader set of lncRNAs, the lnc-pri-miRNA loci as a subset were fourfold enriched for GeneHancer's (34) highly filtered set of double-elite enhancer elements (Fig. 5*B* and *SI Appendix*, Fig. S17*B*). These bioinformatic analyses indicate that in addition to hosting miRNAs, loci that encode lnc-pri-miRNAs are enriched for regulatory elements that are in close three-dimensional (3D) proximity to potential target gene promoters.

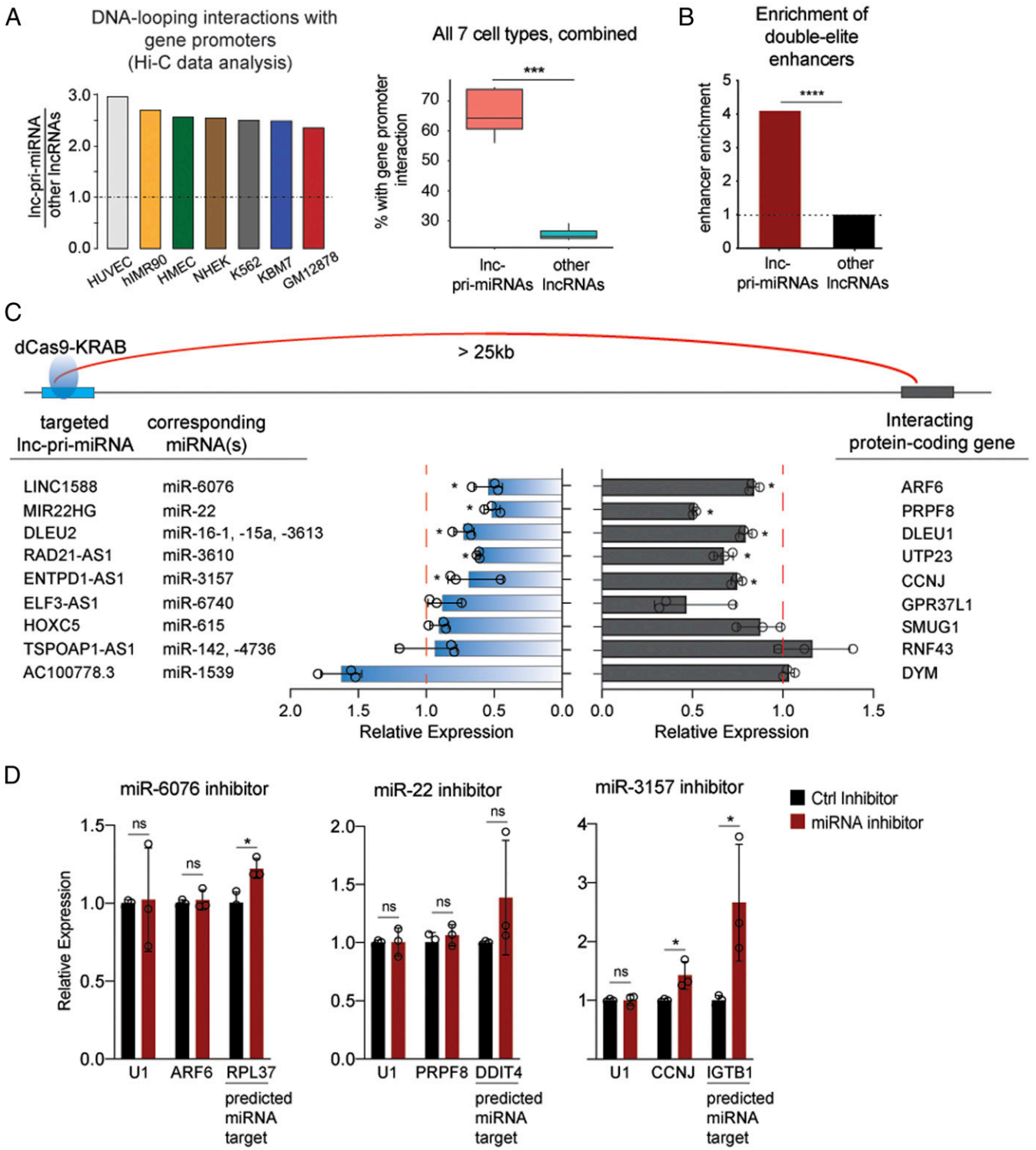

Fig. 5. lnc-pri-miRNAs are enriched for enhancer-like characteristics. (*A*) Enrichment score ratios from genomewide DNA-looping interaction (Hi-C) analysis across seven different cell lines, shown individually (*Left*). Box plot (*Right*) shows the percentage of lnc-pri-miRNAs (or other lncRNAs) that interact with gene promoters in Hi-C data analysis. Horizontal line represents the median, and whiskers represent the interquartile range (***$P < 0.001$, Wilcoxon rank-sum test). (*B*) Enrichment of double-elite enhancer elements in lnc-pri-miRNA loci relative to other lncRNAs (****$P < 0.0001$, Fisher's exact test). (*C*) RT-qPCR quantification of lnc-pri-miRNA levels (blue bars, *Left*) and its interacting protein-coding gene (>25 kb away determined by Hi-C, gray bars, *Right*) 30 h post sgRNA transfection ($n = 3$ biological replicates per condition). Data shown are normalized to Gal4 sgRNA and *U1* controls (*$P < 0.05$, unpaired two-sample *t* test). (*D*) RT-qPCR quantification of K562-dCas9-KRAB cells 48 h after transfection with miRNA inhibitors ($n = 3$ biological replicates per condition). Data shown are normalized to the control inhibitor and *U6*. ns, not significant (*$P < 0.05$, unpaired two-sample *t* test).

lnc-pri-miRNAs can Regulate Local Genes Independent of Its Cognate miRNAs. To investigate whether the physical interaction of lnc-pri-miRNA loci with coding gene promoters predicts enhancer-like function, we individually tested nine lnc-pri-miRNAs that contained GeneHancer double-elite elements and had evidence of physical interactions with coding gene promoters in K562 cells (*SI Appendix*, Fig. S19). We used CRISPRi in K562-dCas9-KRAB cells, targeting the TSS of the lnc-pri-miRNA, and assessed levels of both the lnc-pri-miRNA transcript and the mRNA produced by the gene that interacts with the lnc-pri-miRNA locus, which is >25 kb away (Fig. 5*C*). Of the five lnc-pri-miRNA that had effective knockdown with CRISPRi, all five also exhibited a corresponding decrease of mRNA from the interacting protein-coding gene (Fig. 5*C*). With ChIP, we confirmed H3K9me3 enrichment of all five lnc-pri-miRNA promoters after lnc-pri-miRNA CRISPRi targeting; H3K9me3 was also increased at two of the five interacting protein-coding gene promoters (*SI Appendix*, Fig. S20), which could be an indirect consequence of decreased lnc-pri-miRNA enhancer activity. Next, we used oligonucleotide miRNA inhibitors to investigate whether a reduction in activity of the cognate miRNA caused the decrease in expression of the interacting coding gene. While miRNA inhibitors to miR-6076 (produced by *LINC1588*) caused derepression of a known miR-6076 target gene (*RPL37*), levels of *ARF6* was not decreased (Fig. 5*D*), indicating that a decrease in miR-6076 activity did not indirectly down-regulate *ARF6* expression. Similarly, inhibitors to miR-22 and miR-3157, the cognate miRNAs of lnc-pri-miRNA *MIR22HG* and *ENTPD1*-AS1, respectively, did not decrease expression of their coding gene interacting partners (Fig. 5*D*). Thus, Hi-C/GeneHancer analysis predicts enhancer-like function of lnc-pri-miRNAs, and this activity can be independent of the function of their cognate miRNAs, as observed with *LOC646329* (*SI Appendix*, Fig. S21).

Discussion

In previous studies, the relationship between lnc-pri-miRNAs and their cognate miRNA(s) has been enigmatic. For example, the lnc-pri-miRNA *MIR100HG* produces miR-100 and miR-125b, and these miRNAs drive cetuximab resistance in colorectal cancer cells (8), with *MIR100HG* appearing to function solely as a host for its cognate miRNAs. However, an miRNA-independent role for *MIR100HG* has also been described, as *MIR100HG* knockdown in osteosarcoma cell lines affects the cell cycle without an apparent change in levels of miR-100 or miR-125b (11). Similarly, knockdown of the lnc-pri-miRNA *RMST* inhibits neurogenesis in human cell culture studies without causing an observable change in levels of its cognate miRNA, miR-135a (10). However, other studies demonstrate roles for *miR-135a* in neurogenesis in vivo (12, 37). *PVT1* is another prime example of a lnc-pri-miRNA for which different studies have focused on either miRNA-dependent or miRNA-independent functions (38–41). Such apparent differences in lnc-pri-miRNA function may relate in part to cell type and experimental context.

Neither *DGCR8* nor *DROSHA* knockdown affected the propagation of U87 cells (Fig. 1*D*). All four lnc-pri-miRNA loci CRISPRi screen hits still regulated U87 cell proliferation when *DGCR8* or *DROSHA* were knocked down, even in cells that exhibited no further reduction in mature miRNA levels, suggesting that these lncRNA loci regulate cell biology via miRNA-independent mechanisms. It is important to consider that, while CRISPRi knockdown of lnc-pri-miRNAs in Microprocessor-deficient cells exhibited a cell propagation phenotype, it remains possible that residual miRNA levels could influence cell proliferation. For *LOC646329*, with the miR-29a/b1 cluster being located within an intron ∼36 kb downstream from the TSS, we were able to genetically delete the cluster without apparent detrimental effects to transcription from this locus or its enhancer-like activity. While *LOC646329* did indeed produce miR-29a/b1, which regulated cellular apoptosis, the function of this lnc-pri-miRNA in U87 cell proliferation was miRNA-independent. Thus, in addition to producing miRNAs, lnc-pri-miRNAs can have genetically separable and potent biological function. Of note, without the combination of multiple approaches to dissect miR-29a/b1 from *LOC646329*, the biological effects of *LOC646329* knockdown (and also miR-29a/b1 deletion) might have been attributed solely to the loss of these miRNAs and not the enhancer-like function of this locus.

The *LOC646329* locus is in close 3D proximity to the locus containing *MKLN1* and *linc-PINT*, which is ∼200 kb away. While NRO experiments demonstrated that knockdown of *LOC646329* by ASO-2 can disrupt transcription through the locus, ASO-1 only caused a modest reduction of nascent transcripts at the distal 3′ end. Although ASO-1 did not disrupt transcription through the 5′ end where we observed *LOC646329* enhancer-like activity, it remains possible that this regulatory activity is transcription-dependent, rather than being mediated solely by the RNA transcript itself. ASO-mediated knockdown reduced the interaction frequency between the *LOC646329* promoter and *MKLN1*, suggesting a transcript- or transcription-dependent role in maintaining the observed looping interaction. *MKLN1* is a putative oncogene amplified in human glioma (32) and known to regulate cell adhesion, cytoskeletal dynamics, and cell proliferation (42–44). Interestingly, *MKLN1* levels are not significantly changed in miR-29Δ cells that exhibit increased *LOC646329* expression. *linc-PINT* has also been described to have roles in cancer cell proliferation and invasion (45, 46). Whether the observed regulatory interactions between *LOC646329* and *MKLN1*/*linc-PINT* are derived from a disease state such as GBM (47), and how *linc-PINT* may contribute to GBM pathogenesis, remains to be further investigated. Furthermore, while we have highlighted an enhancer-like activity of *LOC646329*, other lnc-pri-miRNA mechanisms have been described (10, 11). While a variant of *LOC646329* may sponge miR-29b1 in HCT116 colorectal cancer cells (26), we did not find evidence for this lnc-pri-miRNA being an miR-29 target in U87 GBM cells (*SI Appendix*, Figs. S6*B* and S10*A*). Nonetheless, it remains possible that lnc-pri-miRNAs including *LOC646329* can have multiple miRNA-independent functions.

As compared to the broader population of lncRNAs, lnc-pri-miRNAs were enriched for enhancer-like characteristics. For any particular lnc-pri-miRNA, the degree to which miRNA production and enhancer-like activity contributes to the cellular phenotype being studied will likely require detailed molecular-genetic studies of individual loci. For instance, the "essential" function of *LOC646329* in GBM cell proliferation was genetically separable from its production of miR-29a/b1. In K562 cells, Hi-C evidence of 3D "looping" interactions was predictive of enhancer-like activity between lnc-pri-miRNA loci and coding genes, despite these lnc-pri-miRNAs not being scored as hits in screens of cell proliferation. Whether cellular phenotypes are observed with perturbation of lnc-pri-miRNA enhancer-like function may depend upon the assay employed and its sensitivity.

Other lncRNA loci have been previously shown to harbor enhancer-like activity (27, 29–31, 48, 49). *LOC646329* is a distinct example of a lncRNA locus that can function as both a transcriptional enhancer and genetic precursor of miRNAs. This relationship between enhancer-like lncRNA activity and cognate miRNA production, along with the genome-wide enrichment of enhancer-like characteristics within lnc-pri-miRNA loci, suggests a model of genome evolution wherein some miRNAs become embedded into lncRNA loci with enhancer-like activity. That is, while intragenic miRNAs embedded within protein-coding genes may have coevolved function with their "host" genes (50), some intergenic miRNAs (e.g., miR-29a/b1) embedded within lncRNA loci may have coevolved function with the host enhancer-like activity.

Essential lncRNA function is highly cell type-specific (13), and it is unclear how such exquisite functional specificity is achieved.

lncRNA expression alone does not predict function. For instance, human astrocytes express *LOC6436329*, but knockdown of this lnc-pri-miRNA did not reduce cell growth (*SI Appendix*, Fig. S4 *D–F*). Similarly, HeLa cells also express *LOC646329*, and miR-29 regulates apoptosis in this cell line (24). However, *LOC646329* knockdown did not inhibit HeLa cell growth (*SI Appendix*, Fig. S4 *A–C*). For lncRNAs with multiple biological functions such as *LOC646329*, we speculate that each distinct molecular mechanism may play a greater or lesser biological role depending on cell type and/or disease state. For instance, it is possible that, in GBM, the enhancer-like activity of *LOC646329* becomes the dominant function that promotes cell proliferation. Potential differences in the "utilization" of such distinct mechanisms could underlie the apparent cell type specificity of lncRNA function.

Experimental Model and Subject Details

Tissue Culture. We maintained male U87-MG (ATCC cat. no. HTB-14), fetal HEK293T cells (ATCC CRL-3216), female HeLa-dCas9-KRAB, NHA (51) of unknown sex (as no information is reported on the Clonetics Web site), and any U87-derived cells (e.g., miR-29Δ clones) in Dulbecco's modified Eagle medium (Thermo Fisher Scientific), 10% heat-inactivated fetal bovine serum (FBS; VWR), and 1% antibiotic/antimycotic (Thermo Fisher Scientific). K562-dCas9-KRAB cells were maintained in RPMI media with 25 mM Hepes, L-glutamine (Gibco), 10% FBS (VWR), and 1% antibiotic/antimycotic (Thermo Fisher Scientific). All cells were grown at 37 °C and 5% CO_2 atmosphere. The U87-dCas9-KRAB and HeLa-dCas9-KRAB lines were authenticated by BFP expression and effective CRISPRi knockdown. Each of the miR-29Δ cell lines (clones 15, 18, and 40) were authenticated by PCR genotyping, Sanger sequencing, qPCR, and RNA-seq.

Methods

Lentivirus Production. We plated 400,000 293T cells in a six-well plate the day prior to transfecting with 1.35 μg of packaging vector pCMV-dR8.91 (52), 165 ng packaging vector pMD2-G (Addgene plasmid no. 12259), and 1.5 μg of lentiviral plasmid. At 48 h post transfection, we harvested viral supernatants and filtered them through a 0.45-μM syringe filter prior to use.

Spinfection. We plated 300,000 cells in a six-well plate the day prior to transduction. We removed all media prior to transduction and added 1 mL of harvested viral medium containing 8 μg/mL (final concentration) of Polybrene prior to spinning at 2,000 × *g* for 30 min in a centrifuge at room temperature. After spinfection, all viral media is removed and replaced with fresh media. In 2 d, cells were 20 to 30% infected. Puromycin selection can begin (1 μg/mL) for 4 d, with a 2-d recovery. Otherwise, cells can be analyzed by flow cytometry to assess infection efficiency.

ChIP. Cells were fixed using a final concentration of 1% formaldehyde added straight to the culture plates, shaking at room temperature for 10 min. After fixing, cells were quenched with 125 mM (final concentration) glycine, shaking at room temperature for 5 min to stop formaldehyde fixation. Cells were then washed twice using ice-cold phosphate-buffered saline (PBS) solution. Cells were scraped off of the plate using a cell lifter and pelleted for 4 min at 2,000 rpm at 4 °C. Pellet was then thawed and resuspended in cell lysis buffer (5 mM Pipes, pH 8, 86 mM KCl, freshly added 1% octylphenoxypolyethoxyethanol [IGEPAL]) with protease inhibitors (Pierce Halt Protease Inhibitor Mix). Cells were then homogenized using a type B glass Dounce homogenizer, pelleted, and resuspended in nuclei lysis buffer (50 mM Tris·HCl, pH 8, 10 mM ethylenediaminetetraacetic acid [EDTA], 1% sodium dodecyl sulfate [SDS]). Chromatin was incubated on ice for 30 min and then flash-frozen in liquid nitrogen. Next, chromatin was thawed and sonicated in Diagenode TPX tubes using the Diagenode Bioruptor to 150 to 500 bps as determined by gel electrophoresis. Debris was pelleted and discarded, and an aliquot was removed for input DNA sequencing from the sonicated chromatin within the supernatant. Sonicated chromatin was then diluted fivefold in IP dilution buffer (50 mM Tris·HCl, pH 7.4, 150 mM NaCl, 1% IGEPAL, 0.25% deoxycholic acid, 1 mM EDTA, pH 8) with protease inhibitors and precleared with Life Technologies Protein G Dynabeads for 2 h at 4 °C. One microgram of antibody was added per million cells, and samples were incubated overnight at 4 °C. Antibody-bound chromatin was then collected using Life Technologies Protein G Dynabeads and washed twice using IP dilution buffer, twice with IP wash buffer 2 (100 mM Tris·HCl, pH 9, 500 mM LiCl, 1% IGEPAL, 1% deoxycholic acid), once with IP wash buffer 3 (100 mM Tris·HCl, pH 9, 500 mM LiCl, 150 mM NaCl, 1% IGEPAL, 1% deoxycholic acid), and once again with IP wash buffer 3 (100 mM Tris·HCl, pH 9, 500 mM LiCl, 150 mM NaCl, 1% IGEPAL, 1% deoxycholic acid). Precipitated chromatin was then eluted for 30 min at 65 °C with elution buffer (1% SDS, 50 mM $NaHCO_3$). ChIP and input DNA cross-links were reversed by adding 5 M NaCl and heating at 65 °C overnight. The following day, 10 mg/mL RNase A was added to precipitated chromatin, and chromatin was incubated for 30 min at 37 °C. DNA was then recovered using Agencourt AMPure XP Beads and quantified using a Life Technologies Qubit Fluorometer.

Genomewide Pol II ChIP-Seq Analysis. Raw POLR2A ChIP-seq datasets from K562, HUVEC, IMR90, and GM12878 were downloaded from ENCODE and aligned to the human genome (GRCh38 release 95) using hisat2 (v2.1.0). Reads mapping to promoters (defined as 2,000 bp upstream to 200 bp downstream of transcriptional start site) of lnc-pri-miRNAs and all other lncRNAs were determined using featureCounts (subread 2.0.1). ChiP-seq signal at each promoter was determined by calculating the ratio of ChIP reads to input reads at each promoter. All reads were normalized to the total mapped reads for the entire sample. The Wilcoxon rank-sum test was used to determine statistical significance between lnc-pri-miRNA and non–lnc-pri-miRNA lncRNAs.

CRISPRi Chromatin Silencing ChIP-Seq Analysis. Reads were aligned to the hg19 genome using hisat2. Differential H3K9me3 enrichment of gene promoters was performed according to Liu et al. (13) by using featureCounts to quantify mapped reads in a 2-kb window around the TSS and DESeq2 for differential enrichment testing.

Chromatin Isolation by Biochemical Fractionation. Chromatin isolation protocol was performed according to Wysocka et al. (53). We harvested 1×10^7 cells by using a cell scraper and spun them at 1,000 rpm for 2 min prior to discarding the supernatant. Cell pellets were washed twice with PBS, spinning for 2 min at 1,000 rpm between washes. Cells were then resuspended in 200 μL of buffer A (10 mM Hepes, pH 7.9, 10 mM KCl, 1.5 mM $MgCl_2$, 0.34 M sucrose, 10% glycerol, 1 mM dithiothreitol [DTT], Protector RNase Inhibitor [Sigma], and protease inhibitor [Pierce Halt]). After resuspension, Triton X-100 was added to a final concentration of 0.1%. Cells were then incubated on ice for 8 min. The mixture was then centrifuged at 1,300 × *g* at 4 °C for 5 min to separate the supernatant (S1, cytosolic) fraction from the pellet (P1, nuclei) fraction. The supernatant (S1) was further centrifuged at high speed (20,000 × *g*) at 4 °C for 5 min before collecting the supernatant for the final cytosolic (S2) fraction. P1 was washed once with buffer A and lysed with 100 μL of buffer B (3 mM EDTA, 0.2 M ethylene glycol tetraacetic acid, 1 mM DTT, protease inhibitor [Pierce Halt]) for 30 min, then centrifuged at 1,700 × *g* 4 °C for 5 min before supernatant was separated from the pellet (chromatin, P3). The pellet (P3) and S2 could be directly lysed in 1 mL of TRIzol for RNA extraction.

RNA Extraction. Cells (on a plate) or a cell pellet were lysed and harvested using TRIzol (e.g., 300 μL in a single well of a six-well plate). After harvesting with TRIzol, the mixture was prepared and RNA was extracted using the Zymo Direct-zol RNA extraction kit and protocols. RNA concentration was quantified using Nanodrop.

Small RNA Library Preparation for Sequencing. Extracted RNA was prepared following the SMARTer smRNA-Seq Kit (Takara Bio no. 635029) protocol and sequenced with the HiSEq 4000.

Internally Controlled Cell Competition Assay. Lentiviral sgRNA infection was performed at <30% infection efficiency. Treated cells were assessed using flow cytometry 4 d post transduction, and sgRNA-expressing cells (tagged with green fluorescent protein [GFP] or blue fluorescent protein [BFP]) were followed for a period of 2 to 3 wk. A nontargeting sgRNA control was designed to target Gal4. For the *DROSHA* or *DGCR8* double-knockdown experiments, stable U87 CRISPRi cells were selected under puromycin for 4 to 5 d prior to a 2-d recovery to select for stable CRISPRi knockdown of *DROSHA*, *DGCR8*, or Gal4 (GFP^+ vectors) cells. Either Gal4, *DROSHA*, or *DGCR8* CRISPRi knockdown cells were infected with lentiviral sgRNAs targeting control Gal4 or a lnc-pri-miRNA (BFP^+ vectors). Double-knockdown cells were assessed using flow cytometry of cells expressing dual fluorescent tags (BFP^+, GFP^+ cells).

CellTrace Proliferation Assay. CellTrace Violet (5 mM) was prepared by adding 20 μL of dimethyl sulfoxide. A total of 500K cells were plated in a well of a

six-well plate the day prior. At 24 h after plating cells, stock was diluted (5 mM) with CellTrace solution in prewarmed (37 °C) PBS for a final 5-μM solution. The culture media was removed from the cells and replaced with the working solution containing the CellTrace dye, making sure to note complete coverage of the entire well. Cells were incubated at 37 °C, protected from light, for 20 min. The working solution was then removed and washed twice with prewarmed media before replacing the entire well with fresh complete media. The following day, cells were analyzed by flow cytometry to assess uptake and quantification the dye at time point 0. Cells were then followed up to 5 d. With each cell division, fluorescence is reduced in half, thus allowing us to back-calculate and quantify division time.

ASO and miRNA Mimic Transfections. Locked nucleic acid ASOs were designed and purchased from Exiqon. miR-29 mimics were purchased from Dharmacon (C-300521-05-0005 and C-300504-07-0005). These were transfected into cells using Thermo Fisher Scientific Lipofectamine RNAiMAX Reagent under manufacturer's guidelines. A final working concentration of 50 nM was determined effective by titration and used for final experiments.

Immunocytochemistry. Immunostaining was performed using Thermo Fisher Scientific's Click-iT EdU Imaging Kit. Cells were pulsed for 1 h using a final concentration of 10 μM EdU provided by the kit prior to following manufacturer's directions. Cells were blocked for at least 1 h using blocking buffer (50% PBS, 10% normal goat serum, 1% BSA, 0.3% TX-100, 0.3 M glycine final concentrations) prior to incubating with primary antibodies for 2 h in the dark and secondary antibodies for 30 min in the dark. Slides were mounted and dried overnight prior to imaging.

Generation of miR-29 Clones Using CRISPR-Cas9–Mediated Cleavage. U87 cells constitutively expressing Cas9 using the pLentiCas9-T2A-BFP construct (54) were exposed to transient transfection of sgRNAs cloned into the pU6-sgRNA EF1Alpha-puro-T2A-BFP construct (18) for 24 h, followed by a 2-d selection period using 1 μg/mL puromycin. The selected cells were then sparsely plated so single colonies were allowed to form. Each colony was individually and manually picked and plated within a well of a 96-well plate to allow for clonal expansion. *LOC646329-miR29Δ* cells were then confirmed by PCR genotyping, RT-qPCR of mature miR-29a/b1, and derepression of validated miR-29 target genes.

sgRNA Sequences Used. sgRNA sequences used were AGGAAGCTGGTTTCATATGGTGG and CCTAGAGTATACCTTTGATATGG.

CRISPRi. For CRISPRi, cells stably expressing dCas9-KRAB (Addgene plasmid no. 46911) were transduced with sgRNA for 2 d prior to a 4-d puromycin selection and RT-qPCR for confirmation of knockdown. CRISPRi cells were also followed by flow cytometry without selection to track BFP expression in cell competition assays.

sgRNAs used were as follows: sgLOC646329-1, GGACTCAAGACGACCAACAC; sgLOC646329-2, GCACGTGGCTGCCATCTCAG; sgLINC01588, GCACACTAGACGCCAGATGC; sgMIR22HG, GTGGGGGTTGCTGCACGAGG; sgDLEU2, GGCTCCCCGCCCCATCGCCG; sgRAD21-AS1, GACCCTGGGCTGCGGAGGGA; sgENTPD1-AS1, CCGGATATATTGAATCGCCG; sgELF3-AS1, GGGGTACAGGTGGGTCTCAG; sgHOXC5, GACCCATCCTTACAAGACAG; sgTSPOAP1, GGACCAGCTTGGAGTTGTGT; and sgAC100778.3, GAAGCCTCGCCGCGCCCCTT.

RNA FISH. FISH probes were designed and purchased from Advanced Cell Diagnostics (ACD). Cells were plated in Thermo Fisher Scientific Lab-Tek 16-well chamber slides prior to sample preparation using modifications to ACD's fixed frozen tissue using RNAscope Fluorescent Assay.

Modifications were as follows. Part 1, preparation of tissue sections, was skipped. Probes were warmed to 40 °C for 10 min prior to cooling to room temperature and usage. Submerging samples in target retrieval solution was skipped. Protease III treatment was performed by diluting 1:15 and incubating cells in solution for 10 min at room temperature prior to washing off in distilled water and proceeding with the RNAscope Fluorescent Multiplex Kit User Manual Part 2 (doc. no. 320293; https://www.acdbio.com/technical-support/user-manuals.

RNA Half-Life Assessment. Transcription was inhibited by adding 5 μg/mL of actinomycin D to U87 cells, and RNA was harvested at 0, 0.5, 2, and 4 h after treatment before performing RT-qPCR using *GAPDH* for normalization.

Hi-C Data Analysis. The raw mapping Hi-C data for seven cell lines were obtained from the Gene Expression Omnibus (GEO) database (GSE63525) (36). The promoter–promoter/enhancer interactions were identified from Hi-C data using PSYCHIC (35) with 25-Kb resolution window size. The output of PSYCHIC (at a threshold of false discovery rate [FDR] < 1e-2) was intersected with the Gencode transcripts (including lncRNAs and coding genes) before we counted for the calculation of the ratio for lnc-pri-miRNAs/non–lnc-pri-miRNA lncRNAs. The intersections between interactions (at FDR < 1e-2) and lnc-pri-miRNAs/non–lnc-pri-miRNA lncRNAs were performed by using bedtools2-2.26.0. Statistical analysis was performed using the Mann–Whitney test.

GeneHancer Analysis. GeneHancer list of double-elite enhancers (34) was intersected with Gencode v28 database and the annotation of miRNA primary transcript structures from Chang et al. (7). Enhancer enrichment ratio was calculated using the proportion of lnc-pri-miRNAs overlapping double-elite enhancers relative to the proportion of other lncRNAs (non–lnc-pri-miRNAs) overlapping double-elite enhancers. Statistical significance was determined by Fisher's exact test.

Generation of Mammalian DNA-Tag Reporter Vectors. The GFP-tag sequence was PCR-amplified from each of the 13 DNA-tag vectors (55) using primers forward, ATGAGCAAGGGCGAGGAACT, and reverse, CCATGGTGCTGCGCAGATC. The resulting PCR products were individually cloned into a modified pGL4.23 vector (Promega) that already contained a mammalian SCP1 promoter (56). The promoter regions of lncRNA (1 kb upstream and 1 kb downstream from TSS) were PCR-amplified and cloned into the multiple cloning sites upstream of the SP1 promoter. An empty vector without any lncRNA DNA sequence was used as the negative control. Plasmids were transfected into U87 cells, in which plasmids with different tags were mixed at equal molar ratio. The negative control vector was cotransfected in each batch. For ASO knockdown experiments, ASO and enhancer–reporter constructs were cotransfected into the same cells. Cells were collected 48 h after transfection. DNA and RNA were extracted using AllPrep DNA/RNA Micro Kit (Qiagen) following the manufacturer's protocol. qPCR experiments were performed on both DNA and cDNA templates using primers specific to each tag-DNA (55). To calculate the enhancer activity, the relative expression level of each tag compared to the negative control (result from cDNA) was normalized to the amount of transfected DNA (55).

RNA-Seq and Gene Expression Analysis. RNA-seq libraries were prepared using the Illumina TruSeq Stranded mRNA Kit and sequenced on an Illumina HiSEq 4000 system in paired-end mode for 100 cycles with a minimum of 50 million reads per replicate. Read quality assessment, quality trimming, and adapter removal were performed using fastp before aligning to the human reference genome (GRCh38 release 84) with the hisat2 (2.1.0) spliced aligner. Gene expression was quantified using featureCounts (1.5.0), and differentially expressed genes were analyzed using DESeq2 (1.22) in R (3.5) using the likelihood ratio test at an FDR of 0.05. Gene Ontology analysis was performed using Enrichr, with the top 50 genes sorted by "log2 fold change" used as the input list. For genes related to *LOC646329-miR29Δ* knockdown, the top 50 genes sorted by log2 fold change are considered if the genes were also statistically and significantly changed in the "wildtype" *LOC646329* knockdown condition. Predicted target genes of miR-29 were obtained using miRTarBase (57) and TargetScan (58). Small RNA-seq data were aligned using STAR (59).

RNA Isolation, Nanopore Sequencing, and Base Calling. Total RNA was isolated from U87 human glioblastoma cells using TRI Reagent Solution (Thermo Fisher), followed by bead-based poly(A) selection. Approximately 750 ng of poly(A) RNA was used for dT adapter ligation, followed by reverse transcription and additional ligation of motor adapter prior to loading onto the Oxford Nanopore Technologies (ONT) PromethION for sequencing. The ionic current trace for each poly(A) RNA strand is base-called using the ONT Albacore algorithm.

Reduction of miRNA Activity Using mirVana miRNA Inhibitors. Lyophilized inhibitors (5 nmol) to miR-6076, miR-22, miR-15a, miR-16–1, miR-3613, and miR-3157 were ordered from Life Technologies (catalog no. 4464084 with assay IDs MH26155, MH10203, MH10235, MH12371, MH19501, and MH16540, respectively), and negative control inhibitor was catalog no. 4464076. Inhibitor stocks were diluted in nuclease-free water, and 30 pmol of each inhibitor was transfected following the RNAiMAX protocol. Cells were harvested 24 h post transfection for RT-qPCR analysis.

NRO. NRO was performed as described by Lee and Mendell (21) with minor modifications. Five million cells were harvested with trypsin/EDTA, washed with cold PBS, and centrifuged at 4° C for 5 min. The PBS was aspirated and cell pellet resuspended in 500 μL cold lysis buffer (10 mM Hepes, pH 7.4, 10 mM KCl, 1.5 mM $MgCl_2$, 0.34 M sucrose, 0.1% [vol/vol] TX-100, 1 mM DTT) and incubated on ice for 20 min. Samples were centrifuged at 1,300 × *g* for 5 min at 4° C and washed once in 1 mL of cold lysis buffer. The nuclei were then resuspended in 100 μL of cold nuclear storage buffer (50 mM Tris·HCl, pH 8, 0.1 mM EDTA, 5 mM $MgCl_2$, 40% [vol/vol] glycerol) and incubated on ice. Transcription reaction for each sample was prepared with 50 μL of 2× transcription buffer (20 mM Tris·HCl, pH 8, 5 mM $MgCl_2$, 300 mM KCl, 4 mM DTT), 4 μL SUPERase In RNase Inhibitor (20 U/μL; Invitrogen), 1 μL 100 mM BrUTP (Sigma-Aldrich), 2 μL 100 mM ATP (Roche), 2 μL 100 mM GTP (Roche), 2 μL 100 mM CTP (Roche), and 1 μL 100 mM UTP (Roche), mixed well, and combined with nuclei in storage buffer. This reaction (total volume of 100 μL) was mixed by pipetting and incubated at 37° C for 30 min. After 30 min, 600 μL TRIzol LS (Thermo) was added and incubated at room temperature for 5 min. RNA was then isolated using the Zymo mini RNA isolation columns, following manufacturer instructions, with the DNase step. After RNA isolation, bromouridylated RNA was immunoprecipitated: for each sample, 30 μL protein G Dynabeads (Invitrogen) was prewashed in PBST (0.1% [vol/vol] Tween-20 in PBS) and combined with 2 mg of anti-BrdU monoclonal antibody (Santa Cruz Biotechnology). After incubation on a rotating platform for 10 min at room temperature, the beads were washed twice in PBSTR (PBST supplemented with 8 U/μL SUPERase In) and resuspended in 100 μL PBSTR. A total of 2 μg of bromouridylated RNA was denatured at 65° C for 5 min, mixed with the anti-BrdU conjugated beads, and rotated at room temperature for 30 min. Immunocomplexes were magnetically separated and washed three times with PBSTR. To harvest the RNA, 500 μL of TRIzol (Ambion) was added to the beads, mixed by pipetting, and incubated for 5 min at room temperature. A total of 100 μL of chloroform was added, vortexed for 10 s, and incubated for 10 min at room temperature. The samples were then centrifuged at 15,000 rpm for 10 min at 4° C. The aqueous phase was collected and transferred to a new tube. RNA was precipitated by adding 250 μL of isopropanol and 20 μL of GlycoBlue (15 mg/mL; Invitrogen). cDNA was synthesized using the Transcriptor cDNA synthesis kit with random hexamer primers (Roche). Real-time PCR amplification was performed using Fast SYBR Green Master Mix (Life Technologies). Relative quantification of each target, normalized to an endogenous control (*RPLP0*), was performed using the ΔΔCt method.

Chromosome Conformation Capture qPCR. In-nucleus 3C was performed as described in Stadhouders et al. and Nagano et al. (60, 61) with minor modifications. Cells were fixed by adding 37% formaldehyde to a final concentration of 1% and incubating for 10 min at room temperature while tumbling, followed by addition of glycine to a final concentration of 0.125 M to quench. Samples were then centrifuged at 300 × *g* for 8 min at 4 °C, and supernatant was removed. Samples were washed with cold PBS and resuspended in 5 mL ice-cold lysis buffer (10 mM Tris·HCl, pH 8.0, 10 mM NaCl, 0.2% Nonidet P-40, 1× complete protease inhibitor [Roche]), followed by 10 min incubation on ice. Samples were centrifuged at 300 × *g* for 5 min at 4 °C and resuspended in 500 μL 1.2× NEB Buffer 2.1 (B7202S). SDS 20% was added to a final concentration of 0.3%, and samples were incubated for 1 h at 37 °C while shaking at 900 rpm on a thermomixer. Triton X-100 20% was added to a final concentration of 2%, followed by incubation for 1 h at 37 °C while shaking at 900 rpm on a thermomixer. EcoRI (500 U; NEB R0101L) was added to each sample and incubated 20 h at 37 °C while shaking at 900 rpm on a thermomixer. For in-nucleus ligation, 7 mL of ligation mix (820 μL of 10× T4 DNA ligase reaction buffer [NEB], 41 μL of 20 mg/mL bovine serum albumin [NEB B9000S], and rest water) and 10,000 U of T4 DNA Ligase (NEB M0202M) was added per sample. Ligation was performed for 4 to 6 h at 16 °C. De–cross-linking was performed by adding 300 μg proteinase K (Thermo) and incubating for 16 h at 65 °C. RNase (300 μg; Thermo) was added and incubated for 30 min at 37 °C. Samples were purified by phenol:chloroform extraction. Pellets were air-dried and resuspended in 150 μL of 10 mM Tris·HCl (pH 7.5). Digestion efficiency was checked using primer pairs amplifying across EcoRI site using undigested and digested not-ligated aliquots as in Hagège et al. (62). Bacterial artificial chromosome (BAC) clones (RP11-10I12 and RP11-815G13) were ordered from BACPAC Resources and used as control templates to cover the genomic region under study. BAC DNA was digested using 700 U of EcoRI (NEB) at 37 °C overnight. After DNA purification, digested DNA fragments were ligated using T4 DNA ligase (NEB) at 16 °C overnight. DNA was purified by phenol:chloroform and ethanol extraction.

All primers were designed to be within 25 to 100 bp from the nearest restriction enzyme digestion site using the 3C primer design software 3PD. Real-time qPCR was performed using SYBR Green chemistry on a Roche LightCycler 480. The linear range of amplification for templates were determined by serial dilution using titration primers in Naumova et al. (63). To quantify specific chromatin interactions, normalized relative amount of 3C product was calculated using the formula $2^{-\Delta\Delta Ct} = 2^{((Ct\ 3Cinteraction - Ct\ 3Ccontrol) - (Ct\ BACinteraction - Ct\ BACcontrol))}$, where $Ct^{3Cinteraction}$ and $Ct^{BACinteraction}$ quantify PCR products at the test locus in the 3C and BAC template, respectively, and $Ct3^{Ccontrol}$ and $Ct^{BACcontrol}$ quantify PCR product at internal control locus in the 3C and BAC template, respectively.

Data and Materials Availability The datasets generated from this study are publicly available on the GEO repository (GSE137048). The raw and processed imaging datasets generated during this study are publicly available on Mendeley Data (https://dx.doi.org/10.17632/c443rtpbyk.1).

Contact for Reagent and Resource Sharing Further information and requests for reagents should be directed to and will be fulfilled by the lead contact, D.A.L. (daniel.lim@ucsf.edu).

Materials Availability Plasmids generated in this study will be deposited to Addgene. Cell lines will be available upon request.

ACKNOWLEDGMENTS. We would like to acknowledge Josie Hayes, Chibo Hong, and members of the Costello laboratory at the University of California, San Francisco, for their help with the primary and recurrent brain tumor samples. We thank Martina Malatesta for her helpful discussions. This work was supported by NIH Grants 1R01NS091544-01A1, 1R21NS101395-01, 5T32HD007470, and 5T32CA151022P; the Chad Tough Foundation; The Childhood Brain Tumor Foundation; The Boyer Fund; and The Jabsheh Initiative.

1. J. L. Rinn, H. Y. Chang, Long noncoding RNAs: Molecular modalities to organismal functions. *Annu. Rev. Biochem.* **89**, 283–308 (2020).
2. I. Ulitsky, D. P. Bartel, lincRNAs: Genomics, evolution, and mechanisms. *Cell* **154**, 26–46 (2013).
3. H. Wu, L. Yang, L. L. Chen, The diversity of long noncoding RNAs and their generation. *Trends Genet.* **33**, 540–552 (2017).
4. J. J. Quinn, H. Y. Chang, Unique features of long non-coding RNA biogenesis and function. *Nat. Rev. Genet.* **17**, 47–62 (2016).
5. A. Dhir, S. Dhir, N. J. Proudfoot, C. L. Jopling, Microprocessor mediates transcriptional termination of long noncoding RNA transcripts hosting microRNAs. *Nat. Struct. Mol. Biol.* **22**, 319–327 (2015).
6. T. Treiber, N. Treiber, G. Meister, Regulation of microRNA biogenesis and its crosstalk with other cellular pathways. *Nat. Rev. Mol. Cell Biol.* **20**, 5–20 (2019).
7. T. C. Chang, M. Pertea, S. Lee, S. L. Salzberg, J. T. Mendell, Genome-wide annotation of microRNA primary transcript structures reveals novel regulatory mechanisms. *Genome Res.* **25**, 1401–1409 (2015).
8. Y. Lu *et al.*, lncRNA MIR100HG-derived miR-100 and miR-125b mediate cetuximab resistance via Wnt/β-catenin signaling. *Nat. Med.* **23**, 1331–1341 (2017).
9. V. Profumo *et al.*, LEADeR role of miR-205 host gene as long noncoding RNA in prostate basal cell differentiation. *Nat. Commun.* **10**, 307 (2019).
10. S. Y. Ng, G. K. Bogu, B. S. Soh, L. W. Stanton, The long noncoding RNA RMST interacts with SOX2 to regulate neurogenesis. *Mol. Cell* **51**, 349–359 (2013).
11. Q. Sun *et al.*, MIR100 host gene-encoded lncRNAs regulate cell cycle by modulating the interaction between HuR and its target mRNAs. *Nucleic Acids Res.* **46**, 10405–10416 (2018).
12. G. Caronia-Brown, A. Anderegg, R. Awatramani, Expression and functional analysis of the Wnt/beta-catenin induced mir-135a-2 locus in embryonic forebrain development. *Neural Dev.* **11**, 9 (2016).
13. S. J. Liu *et al.*, CRISPRi-based genome-scale identification of functional long noncoding RNA loci in human cells. *Science* **355**, aah7111 (2017).
14. R. I. Gregory *et al.*, The Microprocessor complex mediates the genesis of microRNAs. *Nature* **432**, 235–240 (2004).
15. Y. Wang, R. Medvid, C. Melton, R. Jaenisch, R. Blelloch, DGCR8 is essential for microRNA biogenesis and silencing of embryonic stem cell self-renewal. *Nat. Genet.* **39**, 380–385 (2007).
16. P. Ru *et al.*, Feedback loop regulation of SCAP/SREBP-1 by miR-29 modulates EGFR signaling-driven glioblastoma growth. *Cell Rep.* **16**, 1527–1535 (2016).
17. T. C. Chang *et al.*, Widespread microRNA repression by Myc contributes to tumorigenesis. *Nat. Genet.* **40**, 43–50 (2008).
18. L. A. Gilbert *et al.*, CRISPR-mediated modular RNA-guided regulation of transcription in eukaryotes. *Cell* **154**, 442–451 (2013).
19. L. S. Qi *et al.*, Repurposing CRISPR as an RNA-guided platform for sequence-specific control of gene expression. *Cell* **152**, 1173–1183 (2013).
20. F. Lai, S. S. Damle, K. K. Ling, F. Rigo, Directed RNase H cleavage of nascent transcripts causes transcription termination. *Mol. Cell* **77**, 1032–1043.e4 (2020).

21. J. S. Lee, J. T. Mendell, Antisense-mediated transcript knockdown triggers premature transcription termination. *Mol. Cell* **77**, 1044–1054.e3 (2020).
22. P. B. Rahl *et al*., c-Myc regulates transcriptional pause release. *Cell* **141**, 432–445 (2010).
23. S. Sengupta *et al*., MicroRNA 29c is down-regulated in nasopharyngeal carcinomas, up-regulating mRNAs encoding extracellular matrix proteins. *Proc. Natl. Acad. Sci. U.S.A.* **105**, 5874–5878 (2008).
24. S. Y. Park, J. H. Lee, M. Ha, J. W. Nam, V. N. Kim, miR-29 miRNAs activate p53 by targeting p85 alpha and CDC42. *Nat. Struct. Mol. Biol.* **16**, 23–29 (2009).
25. H. Xu *et al*., miR-29s inhibit the malignant behavior of U87MG glioblastoma cell line by targeting DNMT3A and 3B. *Neurosci. Lett.* **590**, 40–46 (2015).
26. A. R. Javanmard, S. Dokanehiifard, M. Bohlooli, B. M. Soltani, LOC646329 long non-coding RNA sponges miR-29b-1 and regulates TGFβ signaling in colorectal cancer. *J. Cancer Res. Clin. Oncol.* **146**, 1205–1215 (2020).
27. J. M. Engreitz *et al*., Local regulation of gene expression by lncRNA promoters, transcription and splicing. *Nature* **539**, 452–455 (2016).
28. S. Luo *et al*., Divergent lncRNAs regulate gene expression and lineage differentiation in pluripotent cells. *Cell Stem Cell* **18**, 637–652 (2016).
29. U. A. Ørom *et al*., Long noncoding RNAs with enhancer-like function in human cells. *Cell* **143**, 46–58 (2010).
30. K. C. Wang *et al*., A long noncoding RNA maintains active chromatin to coordinate homeotic gene expression. *Nature* **472**, 120–124 (2011).
31. C. A. Melo *et al*., eRNAs are required for p53-dependent enhancer activity and gene transcription. *Mol. Cell* **49**, 524–535 (2013).
32. H. Nord *et al*., Characterization of novel and complex genomic aberrations in glioblastoma using a 32K BAC array. *Neuro-oncol.* **11**, 803–818 (2009).
33. H. Won *et al*., Chromosome conformation elucidates regulatory relationships in developing human brain. *Nature* **538**, 523–527 (2016).
34. S. Fishilevich *et al*., GeneHancer: Genome-wide integration of enhancers and target genes in GeneCards. *Database (Oxford)* **2017**, bax028 (2017).
35. G. Ron, Y. Globerson, D. Moran, T. Kaplan, Promoter-enhancer interactions identified from Hi-C data using probabilistic models and hierarchical topological domains. *Nat. Commun.* **8**, 2237 (2017).
36. S. S. Rao *et al*., A 3D map of the human genome at kilobase resolution reveals principles of chromatin looping. *Cell* **159**, 1665–1680 (2014).
37. M. Pons-Espinal *et al*., MiR-135a-5p is critical for exercise-induced adult neurogenesis. *Stem Cell Reports* **12**, 1298–1312 (2019).
38. Y. Y. Tseng *et al*., PVT1 dependence in cancer with MYC copy-number increase. *Nature* **512**, 82–86 (2014).
39. S. W. Cho *et al*., Promoter of lncRNA gene PVT1 is a tumor-suppressor DNA boundary element. *Cell* **173**, 1398–1412.e22 (2018).
40. G. Papagregoriou *et al*., A miR-1207-5p binding site polymorphism abolishes regulation of HBEGF and is associated with disease severity in CFHR5 nephropathy. *PLoS One* **7**, e31021 (2012).
41. C. Yan *et al*., PVT1-derived miR-1207-5p promotes breast cancer cell growth by targeting STAT6. *Cancer Sci.* **108**, 868–876 (2017).
42. F. Lampert *et al*., The multi-subunit GID/CTLH E3 ubiquitin ligase promotes cell proliferation and targets the transcription factor Hbp1 for degradation. *eLife* **7**, e35528 (2018).
43. O. Francis, F. Han, J. C. Adams, Molecular phylogeny of a RING E3 ubiquitin ligase, conserved in eukaryotic cells and dominated by homologous components, the muskelin/RanBPM/CTLH complex. *PLoS One* **8**, e75217 (2013).
44. C. F. Delto *et al*., The LisH motif of muskelin is crucial for oligomerization and governs intracellular localization. *Structure* **23**, 364–373 (2015).
45. J. Duan *et al*., Long noncoding RNA *LINC-PINT* promotes proliferation through EZH2 and predicts poor prognosis in clear cell renal cell carcinoma. *OncoTargets Ther.* **12**, 4729–4740 (2019).
46. O. Marín-Béjar *et al*., The human lncRNA LINC-PINT inhibits tumor cell invasion through a highly conserved sequence element. *Genome Biol.* **18**, 202 (2017).
47. W. A. Flavahan *et al*., Insulator dysfunction and oncogene activation in IDH mutant gliomas. *Nature* **529**, 110–114 (2016).
48. F. Lai *et al*., Activating RNAs associate with Mediator to enhance chromatin architecture and transcription. *Nature* **494**, 497–501 (2013).
49. W. Li *et al*., Functional roles of enhancer RNAs for oestrogen-dependent transcriptional activation. *Nature* **498**, 516–520 (2013).
50. G. S. França, L. C. Hinske, P. A. Galante, M. D. Vibranovski, Unveiling the impact of the genomic architecture on the evolution of vertebrate microRNAs. *Front. Genet.* **8**, 34 (2017).
51. Y. Sonoda *et al*., Formation of intracranial tumors by genetically modified human astrocytes defines four pathways critical in the development of human anaplastic astrocytoma. *Cancer Res.* **61**, 4956–4960 (2001).
52. S. A. Stewart *et al*., Lentivirus-delivered stable gene silencing by RNAi in primary cells. *RNA* **9**, 493–501 (2003).
53. J. Wysocka, P. T. Reilly, W. Herr, Loss of HCF-1-chromatin association precedes temperature-induced growth arrest of tsBN67 cells. *Mol. Cell. Biol.* **21**, 3820–3829 (2001).
54. C. Pulido-Quetglas *et al*., Scalable design of paired CRISPR guide RNAs for genomic deletion. *PLOS Comput. Biol.* **13**, e1005341 (2017).
55. J. Nam, P. Dong, R. Tarpine, S. Istrail, E. H. Davidson, Functional cis-regulatory genomics for systems biology. *Proc. Natl. Acad. Sci. U.S.A.* **107**, 3930–3935 (2010).
56. T. Juven-Gershon, S. Cheng, J. T. Kadonaga, Rational design of a super core promoter that enhances gene expression. *Nat. Methods* **3**, 917–922 (2006).
57. C. H. Chou *et al*., miRTarBase update 2018: A resource for experimentally validated microRNA-target interactions. *Nucleic Acids Res.* **46**, D296–D302 (2018).
58. V. Agarwal, G. W. Bell, J. W. Nam, D. P. Bartel, Predicting effective microRNA target sites in mammalian mRNAs. *eLife* **4**, e05005 (2015).
59. A. Dobin *et al*., STAR: Ultrafast universal RNA-seq aligner. *Bioinformatics* **29**, 15–21 (2013).
60. R. Stadhouders *et al*., Multiplexed chromosome conformation capture sequencing for rapid genome-scale high-resolution detection of long-range chromatin interactions. *Nat. Protoc.* **8**, 509–524 (2013).
61. T. Nagano *et al*., Comparison of Hi-C results using in-solution versus in-nucleus ligation. *Genome Biol.* **16**, 175 (2015).
62. H. Hagège *et al*., Quantitative analysis of chromosome conformation capture assays (3C-qPCR). *Nat. Protoc.* **2**, 1722–1733 (2007).
63. N. Naumova, E. M. Smith, Y. Zhan, J. Dekker, Analysis of long-range chromatin interactions using Chromosome Conformation Capture. *Methods* **58**, 192–203 (2012).